

## Abstract #551

G-CASPR and VDRad: extreme cases of a continuum. Intermediate may be better.

A. Godino-Moya, J. Royuela-del-Val, R.M. Menchón-Lara, M. Martín-Fernández, C. Alberola-López  
Valladolid, ES, University of Valladolid, Image Processing Lab

Preclinical Studies and Basic Science » Image analysis  
Scientific Session

### Purpose / Introduction

Different approaches that use Cartesian trajectories with spiral profiles and golden angle step have been proposed to accelerate MRI acquisition. G-CASPR<sup>[1]</sup> is characterized by a scheme with uniform k-space sampling and it is usually applied to static MRI, but in <sup>[2]</sup> it is used in cardiac cine. Nevertheless, compressed sensing shows better results if the center of k-space is sampled more densely<sup>[3,4]</sup>. VDRad<sup>[5]</sup> is a variable density sampling scheme that has been reported for abdominal imaging. VDRad, however, has the drawback that some positions in the k-space are repeatedly acquired, decreasing efficiency. We define a versatile sampling scheme that varies continuously from the G-CASPR to VDRad. Our goal is to determine whether intermediate configurations can provide better sampling schemes for cine cardiac MRI applications.

### Subjects and Methods

The proposed sampling scheme is described as follows: given a spiral length  $L$ , the  $(K_x, K_y)$ -plane is divided into  $L$  elliptical rings and each ring in turn is divided in  $L$  sectors. Rings can have constant area, constant radial width or something in between, which is controlled by the parameter  $\alpha$  (Figure1).  $\alpha=0$  produces rings with the same number of samples (equivalent to G-CASPR), whereas  $\alpha=1$  produces rings with different number of samples (equivalent to VDRad). Samples within each ring are ordered by radius and by angle in the k-space. Trajectories are formed by choosing each time one sample of one ring and sector forming a spiral twist. Resulting spirals are ordered according to the golden angle  $137.5^\circ$ . The number of the total acquired samples is adjusted by the desired acceleration factor. Images were reconstructed using kt-SPARSE-SENSE with temporal total variation<sup>[6]</sup>. One slice of real data from a regular fully sampled, Cartesian breath hold acquisition with 32 coils was used to test our method. SER and HF-SER<sup>[7]</sup> were calculated to measure image reconstruction quality.

### Results

Figure2 shows the SER and HF-SER for a 2D image reconstruction with different AF and  $\alpha$ -values. The plot seems coherent with the reconstructions included in Figure3. Differences, albeit subtle, can be appreciated (highlighted with arrows).

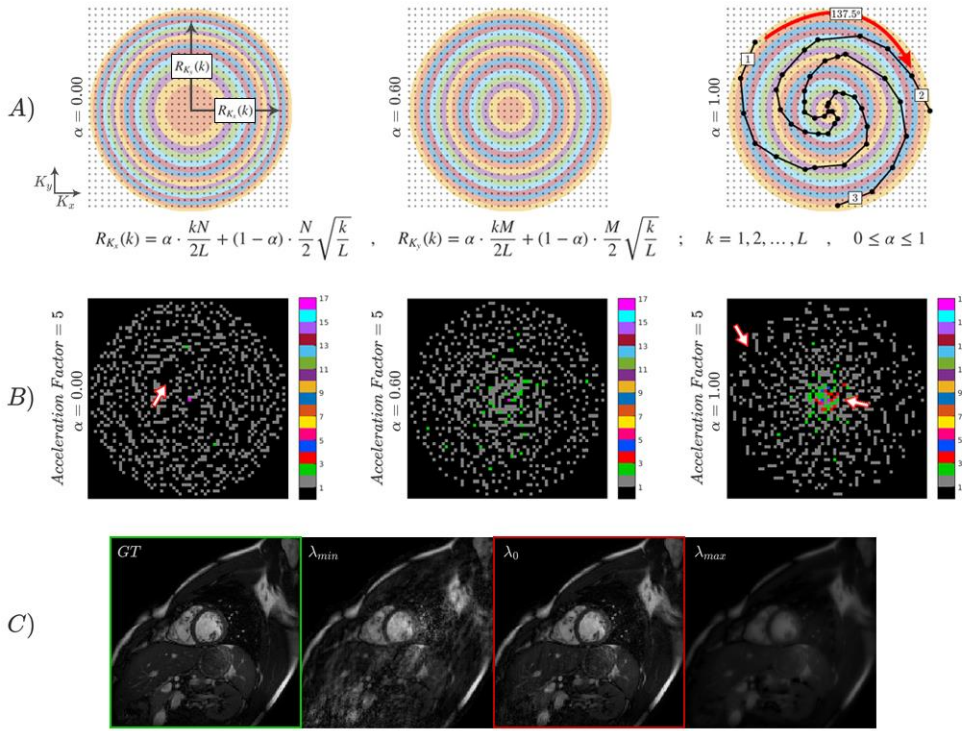


Figure 1: proposed method overview: A)  $(K_x, K_y)$ -plane is divided into rings. Each ring radius is calculated according to the equations indicated.  $R_{K_x}(k)$  and  $R_{K_y}(k)$  are the radii of the  $k$ -th ring in the  $K_x$  and  $K_y$  directions, respectively.  $L$  is the number of samples per spiral and  $N \times M$  is the size of the image. In the figure,  $N=M$  and, therefore, circles are represented. Consecutive spirals are separated an angle given by the golden ratio. On the left, each ring has the same area ( $\alpha=0.00$ ), on the right each ring has the same radial width ( $\alpha=1.00$ ). In the center an intermediate case is shown ( $\alpha=0.60$ ) where each ring has variable radial width and area. B) Resulting sampling patterns for different values of  $\alpha$  after the cardiac binning. Sampling patterns show uniformity for  $\alpha=0$ , although there are some zones with a few samples in the center of  $k$ -space. The density in the center of  $k$ -space increases progressively with the value of  $\alpha$  and so do the repetitions of samples. The number of times that a sample has been visited is represented by colors. C) Reconstructions for different values of the regularization parameter  $\lambda$ . Green frame: ground truth image. Red frame: reconstructed image with empirically selected value of  $\lambda$ .

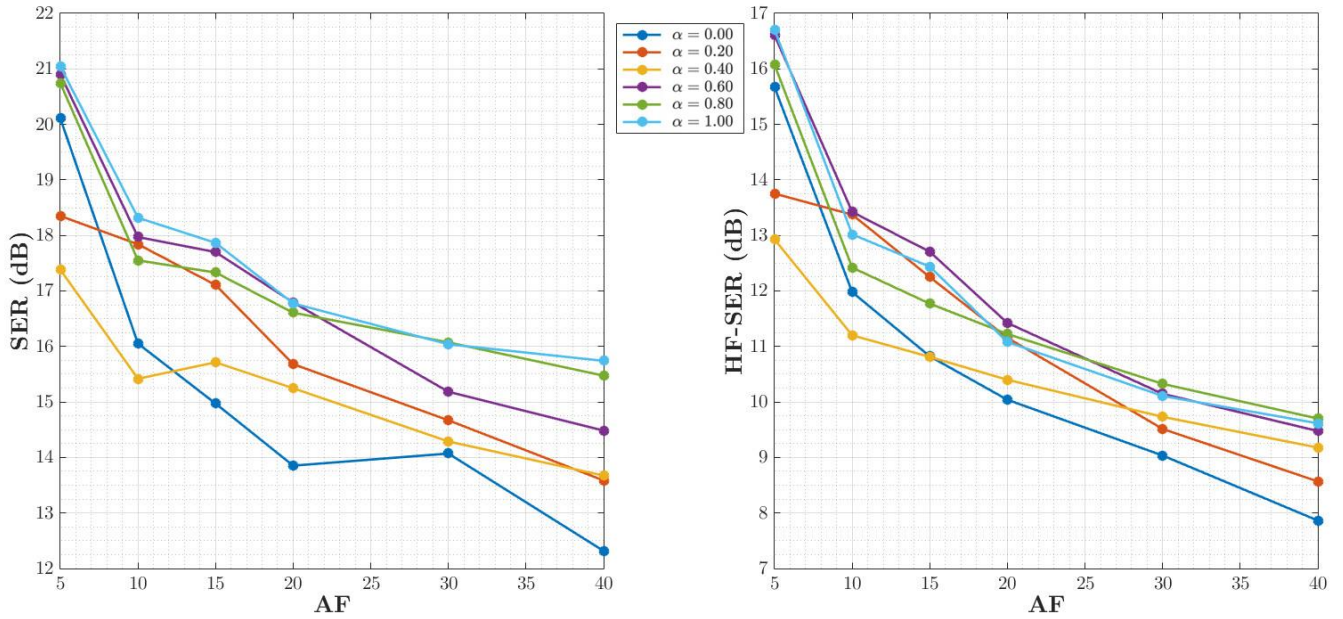


Figure 2: results for 2D image reconstruction with different AFs; each curve is parameterized by the value of  $\alpha$  employed. The figure on the left hand side shows the values of SER. The figure on the right hand side shows the values of HF-SER for the same AFs and values of  $\alpha$ . HF-SER is a specialized quality measure in which the sharpness of boundaries plays a higher role.

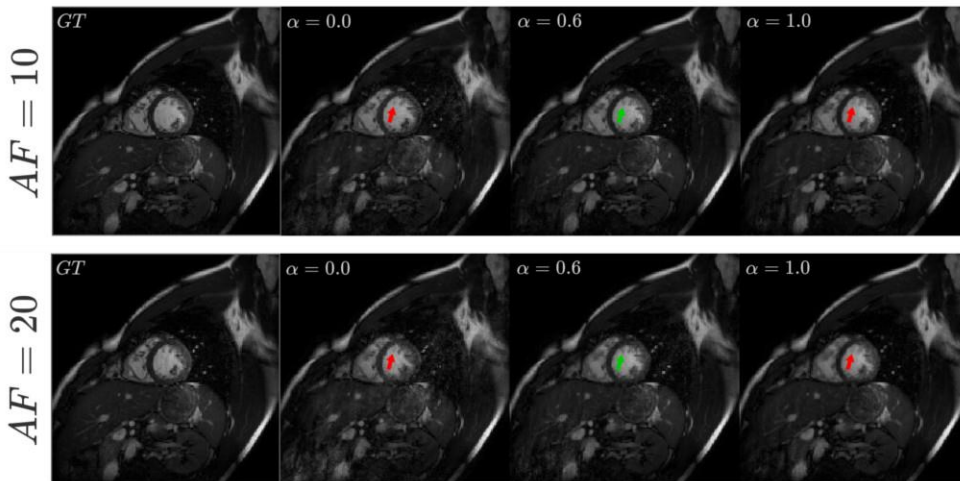


Figure 3: reconstructed images for different values of AF and  $\alpha$ . Two AFs have been used and we show three values of  $\alpha$  (the two extremes and the best intermediate  $\alpha$  for those AFs, i.e.,  $\alpha=0.6$ ). Green arrows point significant locations with better quality than red ones. Ground truth is included for easier reference. Images for  $\alpha=1.0$  show more blurring than with intermediate  $\alpha$ -values and some structures are more clearly revealed with these values, which agrees with HF-SER graphic in Figure 2.

## Discussion / Conclusion

We have developed a variable sampling scheme that allows, by means of a continuous parameter, to select from uniform sampling of k-space to denser sampling in its center. The extremes cases ( $\alpha=0$ ,  $\alpha=1$ ) are not necessarily the best choice, as we have shown in Figure3 and quantified in Figure2.

## Acknowledgements

The authors acknowledge funds form MINECO and Junta de Castilla y León through grants TEC2014-57428-R and VA069U16, respectively.

## References

- [1] C. Prieto et al., "Highly efficient respiratory motion compensated free-breathing coronary MRA using golden-step Cartesian acquisition," *J. Magn. Reson. Imaging*, vol. 41, no. 3, pp. 738–746, 2015.
- [2] M. Usman et al., "Free breathing whole-heart 3D CINE MRI with self-gated Cartesian trajectory," *Magn. Reson. Imaging*, vol. 38, pp. 129–137, 2017.
- [3] Lustig, M., Donoho, D. and Pauly, J. M. (2007), Sparse MRI: The application of compressed sensing for rapid MR imaging. *Magn. Reson. Med.*, 58: 1182–1195.
- [4] B. Adcock et al., "Generalized sampling: Stable reconstructions, inverse problems and compressed sensing over the continuum," *Adv. Imaging Electron Phys.*, vol. 182, pp. 187–279, 2014.
- [5] J. Y. Cheng et al., "Free-breathing pediatric MRI with nonrigid motion correction and acceleration," *J. Magn. Reson. Imaging*, vol. 42, no. 2, pp. 407–420, 2015.
- [6] L. Feng et al., "Highly accelerated real-time cardiac cine MRI using k-t SPARSE-SENSE," *Magn. Reson. Med.*, vol. 70, no. 1, pp. 64–74, 2013.
- [7] G. Cruz et al., "Accelerated motion corrected three-dimensional abdominal MRI using total variation regularized SENSE reconstruction," *Magn. Reson. Med.*, vol. 75, no. 4, pp. 1484–1498, 2016.